

# Experimental constraint on axion-like particle coupling over seven orders of magnitude in mass

Tanya S. Roussy,<sup>1,2,\*</sup> Daniel A. Palken,<sup>1,2</sup> William B. Cairncross,<sup>1,2,†</sup> Benjamin M. Brubaker,<sup>1,2</sup>  
Daniel N. Gresh,<sup>1,2,‡</sup> Matt Grau,<sup>1,2,§</sup> Kevin C. Cossel,<sup>1,2,¶</sup> Kia Boon Ng,<sup>1,2</sup> Yuval Shagam,<sup>1,2</sup>  
Yan Zhou,<sup>1,2,\*\*</sup> Victor V. Flambaum,<sup>3,4</sup> Konrad W. Lehnert,<sup>1,2</sup> Jun Ye,<sup>1,2</sup> and Eric A. Cornell<sup>1,2</sup>

<sup>1</sup>*JILA, NIST and University of Colorado, Boulder, Colorado 80309, USA*

<sup>2</sup>*Department of Physics, University of Colorado, Boulder, Colorado 80309, USA*

<sup>3</sup>*School of Physics, University of New South Wales, Sydney 2052, Australia*

<sup>4</sup>*Johannes Gutenberg University of Mainz, 55128 Mainz, Germany*

(Dated: July 2, 2020)

We use our recent electric dipole moment (EDM) measurement data to constrain the possibility that the  $\text{HfF}^+$  EDM oscillates in time due to interactions with candidate dark matter axion-like particles (ALPs). We employ a Bayesian analysis method which accounts for both the look-elsewhere effect and the uncertainties associated with stochastic density fluctuations in the ALP field. We find no evidence of an oscillating EDM over a range spanning from 27 nHz to 400 mHz, and we use this result to constrain the ALP-gluon coupling over the mass range  $10^{-22} - 10^{-15}$  eV. This is the first laboratory constraint on the ALP-gluon coupling in the  $10^{-17} - 10^{-15}$  eV range, and the first laboratory constraint to properly account for the stochastic nature of the ALP field.

A measurement of the permanent electric dipole moment of the electron (eEDM,  $d_e$ ) well above the standard model prediction of  $|d_e| \leq 10^{-38} e \text{ cm}$  would be evidence for new physics [1–5]. The search for permanent EDMs of fundamental particles was launched by Purcell and Ramsey in the 1950s [6, 7], but it was not until recently that physicists began to consider the possibility of *time-varying* EDMs inspired in large part by hypothetical axion-like particles (ALPs) [8–13]. Coupling to ALPs can cause EDMs of paramagnetic atoms and molecules to vary, due to variations in  $d_e$  or the scalar-pseudoscalar nucleon-electron coupling  $C_S$ . In this paper, we extend our analysis of the EDM data we collected in 2016 and 2017 [14] to place a limit on the possibility that  $C_S$  oscillates in time. This allows us to put a constraint on the hypothetical ALP-gluon coupling over seven orders of magnitude in mass.

Dark matter is one of the largest unsolved mysteries in modern physics: the microscopic nature of 84% of our universe’s cosmic matter density remains inscrutable [15]. A family of candidate dark matter particles, referred to as axion-like particles, are pseudoscalar fields favored for their potential role in solving problems such as the strong CP problem, baryogenesis, the cosmological constant, and small-scale cosmic structure formation [16]. ALPs can be anything from the QCD axion [17–20] to ultralight axions from string theory [21], with different models favouring different mass ranges [16, 22–26]. In this paper, we will consider ultralight spin-0 bosonic fields whose mass  $m_a$  can range from  $10^{-24} - 10^1$  eV (or  $10^{-10} - 10^{15}$  Hz) [26]. ALPs in the low end of this mass range would solve some issues pertaining to small scale structure raised by astrophysical results [16, 25, 27, 28].

Ultralight dark matter particles such as these must be bosonic — the observed matter density can’t be reproduced with light fermions because their Fermi velocity

would exceed the galactic escape velocity. The result is a field with high mode occupation, well described classically as a wave, oscillating primarily at the Compton frequency  $\nu = m_a c^2 / h$ . Astrophysical observations tell us that a quasi-Maxwellian dark matter velocity distribution would have, near earth, a dispersion of  $\delta v \sim 10^{-3} c$ , which in turn leads to a coherence for the dark matter (DM) wave of about  $10^6$  cycles [29]. This finite linewidth ultimately limits the sensitivity of any experiment whose total observation time approaches or exceeds the coherence time.

Several distinct couplings to ALP fields can result in an oscillating CP-odd quantity such as  $d_e$  or  $C_S$ , which amounts to an oscillating molecular EDM signal in our data. The most straightforward effect is the derivative coupling of the ALP field to the pseudovector electron current operator — in other words, a direct coupling between ALP and electron. Unfortunately, in an atomic or molecular system the observable effect scales linearly with  $m_a$ , leading to a large suppression for the mass range we explore [13]. A second potential coupling is from the ALP-induced modification of the electron-nucleon Coulomb interaction [12]. Regrettably, the nature of this effect has not been elucidated in detail, but it is also expected to scale linearly with  $m_a$  [30]. Finally, there are two distinct effects due to the coupling of ALPs to gluons. The first leads to a partially screened nuclear EDM which would be enhanced in polar molecules but scales linearly with  $m_a$ , which again is problematic in the mass range we probe [31]. The second effect will result in an oscillating  $C_S$  and this is independent of  $m_a$  [32–34]. In this paper, we use the hypothesized oscillation in  $C_S$  to constrain the ALP-gluon coupling.

To understand the analysis discussed herein, the reader should be familiar with a few key details from the original measurement. Complete details can be found in

[14] and references therein. The heart of our experiment is an electron spin precession measurement of  $^{180}\text{Hf}^{19}\text{F}^+$  molecular ions confined in a radio-frequency Paul trap and polarized in a rotating bias field to extract the relativistically-enhanced CP-violating energy shift  $2hW_S C_S$  between the stretched and oriented  $m_F \Omega$  Stark sublevels [35]. The molecule-specific structure constant  $W_S = 20.4$  kHz [36],  $h$  is Planck's constant, and we assume for the remainder of this paper that  $d_e$  is zero. Our experimental signal is a count of  $\text{Hf}^+$  ions generated by state-selective dissociation of the  $\text{HfF}^+$  ions. From this signal we generate an asymmetry  $\mathcal{A}'_i = \pm \frac{N_i - \langle \text{Hf}^+ \rangle}{\langle \text{Hf}^+ \rangle}$ . Here,  $N_i$  is the  $\text{Hf}^+$  count in a single *shot* (run) of the experiment and  $\langle \text{Hf}^+ \rangle$  is the mean  $\text{Hf}^+$  count for the *data point* (set of shots, averaged) to which the shot belongs. The sign of  $\mathcal{A}'_i$  is given by the spin preparation/readout conditions [37, 38]. A set of asymmetries, taken by sandwiching a variable free-evolution time  $t_R$  between 2 coherent  $m_F$  mixing pulses, generates a Ramsey fringe. The frequency of the Ramsey fringe is directly proportional to the energy difference between the  $m_F = \pm 3/2$  states in a given Stark doublet.

The Ramsey fringe frequency has multiple contributions:

$$f_R = 3g_F \mu_B B_{\text{rot}}/h + 3\alpha' f_{\text{rot}} \tilde{R}\tilde{B} - 2W_S C_S \tilde{D}\tilde{B} + \dots, \quad (1)$$

where  $g_F$  is the  $F = 3/2$  state g-factor,  $\mu_B$  is the Bohr magneton,  $B_{\text{rot}}$  is the magnitude of the rotating bias magnetic field,  $f_{\text{rot}}$  is the frequency of rotation,  $\tilde{B}$  is the sign of the magnetic field,  $\tilde{D}$  is the populated Stark doublet,  $\tilde{R}$  is the sense of the electric bias field rotation, and  $\alpha'$  is a parameter describing Berry's phase [39]. For any given measurement, the experiment will be in a given *switch state*, characterized by the values of  $\{\tilde{B}, \tilde{D}, \tilde{R}\} = \{\pm 1, \pm 1 \pm 1\}$ . To isolate the CP-violating energy  $2hW_S C_S$ , we repeat our spin precession measurement in each of the  $2^3$  unique states at varying free-evolution times to form eight different Ramsey fringes and respective *switch frequency* measurements  $f^{\{\tilde{B}\tilde{D}\tilde{R}\}}$ . From each set of eight fringes (called a *block*) we form linear combinations of our measured switch frequencies to form *parity frequencies*:  $\mathbf{f}^{\text{parity}} = M^{-1} \mathbf{f}^{\{\tilde{B}\tilde{D}\tilde{R}\}}$ , where  $M^{-1}$  is a transformation matrix and  $\mathbf{f}$  indicates the set of parity or switch frequencies. One of these linear combinations isolates, to first order, the CP-violating  $C_S$  term  $f^{C_S} = 2W_S C_S$ .

Because we collect our data in blocks, this analysis is broken into two parts: ‘low frequency’ (27 nHz – 126  $\mu\text{Hz}$ ) and ‘high frequency’ (126  $\mu\text{Hz}$  – 400 mHz) [40, 41]. In the low frequency analysis, we simply take the  $f^{C_S}$  measurement from each block as a function of block acquisition time (see [41], Figure 1) and reanalyze the data to check for oscillations in our signal. In the high frequency analysis we break apart each block and fringe

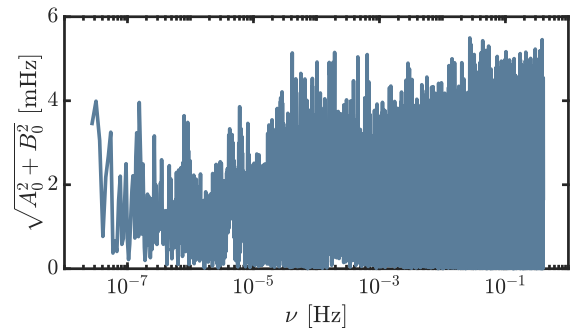


FIG. 1. Least-squares spectral analysis of our EDM data.

to extract a (potentially) time-varying  $C_S$  signal from each shot of the experiment, allowing us to extend the bandwidth of our search over an additional three orders of magnitude.

The low frequency analysis begins with least-squares spectral analysis (LSSA) on our set of  $f^{C_S}$  measurements as a function of block acquisition time. We minimize

$$\chi^2 = \sum_{i=1}^N \frac{1}{\sigma_i^2} [A \cos(\omega T_i) + B \sin(\omega T_i) - f^{C_S}(T_i)]^2 \quad (2)$$

over  $A$  and  $B$  for every potential ALP oscillation frequency  $\nu = \omega/(2\pi)$  of interest, where  $\sigma_i$  is the standard error on a given  $f^{C_S}$  measurement and  $T_i$  is the block acquisition time in seconds with respect to the temporal center of the dataset. This equation is analytically solvable, so we directly compute the minima of the resulting quadratic equation to obtain the ‘best fit’ values of  $A$  and  $B$ :  $A_0(\nu)$  and  $B_0(\nu)$ .

For our high frequency analysis we want to perform LSSA directly on the set of asymmetry measurements as a function of shot acquisition time  $T$ . It may be helpful at this point to emphasize that we have two different time streams: the *free-evolution time*  $t_R$  (often  $\sim 0.5 - 0.7$  seconds) which is an entirely distinct parameter from the *shot/data acquisition time*  $T$  (which ranges between  $\pm 2 \cdot 10^7$  seconds). The asymmetry measurements already oscillate as a function of free-evolution time ( $t_R$ ), and for a static (DC) EDM measurement it is assumed this oscillation frequency is constant (for a given switch state, up to experimental noise). In the presence of an oscillating  $f^{C_S}(T)$ , however, we expect the already-present oscillation in  $t_R$  to be frequency modulated in  $T$ , and we need to determine the form of this frequency modulation. We begin with the fits generated from our DC analysis in [14]: the asymmetry points  $\mathcal{A}'(t_R)$  from each fringe in a given switch state were fit to  $\mathcal{A}'^{\text{fit}}(t_R) = -C e^{-\gamma t_R} \cos(2\pi f_R t_R + \phi) + O$ , where  $C$  is the fringe contrast,  $f_R$  is the fringe frequency,  $\phi$  is the initial phase,  $O$  is the offset, and  $\gamma$  is the coherence decay rate. As mentioned earlier, the frequency  $f_R$  measured in a given fringe does not provide a direct measurement of  $C_S$ ; it contains multiple contributions. The frequency

due to non- $C_S$  terms is  $f_0 = f_R - M' f^{C_S}$ , where  $M'$  are the matrix elements used to transform between switch and parity bases and  $f^{C_S}$  is the frequency component due to  $C_S$ . Since we are only interested in the potentially time-varying  $C_S$  component (and we assume it has a mean of zero [14]) we write

$$\begin{aligned} f_R(T) &= f_0 + M' f^{C_S}(T), \\ f^{C_S}(T) &= A \cos(\omega T) + B \sin(\omega T). \end{aligned} \quad (3)$$

If we include this frequency modulation (which we assume is very small), we can expand our fit asymmetry  $\mathcal{A}^{\text{fit}}$  to second order in  $f^{C_S}(T)$  to obtain

$$\begin{aligned} \mathcal{A}^{\text{osc}}(T) &= -C e^{-\gamma t_R} \cos(2\pi(f_0 + M' f^{C_S}(T))t_R + \phi) + O \\ &\sim -C e^{-\gamma t_R} \cos(2\pi f_0 t_R + \phi) + O \\ &+ C e^{-\gamma t_R} (2\pi t_R M' f^{C_S}(T)) \sin(2\pi f_0 t_R + \phi) \\ &+ C e^{-\gamma t_R} 2(\pi t_R M' f^{C_S}(T))^2 \cos(2\pi f_0 t_R + \phi), \end{aligned} \quad (4)$$

which is our desired expression for the  $f^{C_S}(T)$ -induced frequency modulation. With this, we perform LSSA on the difference between  $\mathcal{A}^{\text{osc}}(T)$  and  $\mathcal{A}'(T)$ ,

$$\chi^2 = \sum_{i=1}^N \frac{1}{\sigma_i^2} [\mathcal{A}_i^{\text{osc}} - \mathcal{A}'_i]^2, \quad (5)$$

where the subscript indicates the  $i^{\text{th}}$  acquisition time point in our dataset.

Combined with the results for the low frequency analysis, we obtain a measure of the ‘‘best fit’’ oscillation amplitude over seven orders of magnitude (Figure 1). Now we can ask: to what extent do our fit values convince us that  $C_S$  is *actually* oscillating, given experimental noise and the look-elsewhere effect [42]? To answer this question we used the Bayesian Power Measured (BPM) analysis framework developed by Palken et al. [43].

The essence of the BPM framework is a comparison between the probability of measuring a given oscillation amplitude assuming the existence of an ALP with a specified mass and coupling and the probability of measuring the same amplitude assuming it doesn’t exist. This means we need probability distributions for both cases at each frequency  $\nu$ , which we can evaluate at the actual measured values  $A_0, B_0$ . For the case where ALPs do not exist, we get the distributions by generating simulated data which by construction has no coherent  $C_S$  oscillation in it. For the low frequency data we generate a single point of ‘noise’ at each acquisition time in the real dataset. Each point of noise is drawn from a Gaussian distribution with mean of zero and a variance which matches that of the real dataset. For the high frequency analysis we randomly shuffle the timestamps of the actual asymmetry measurements in such a manner as to effectively erase any coherent oscillation which may be present in the  $C_S$  channel while preserving both the basic structure of the data (including the general coherent

oscillation present in each fringe) and the technical noise (see [41] for more details).

Once we have this simulated data we perform LSSA on it to get ‘‘best fit’’ values for  $A, B$  at each frequency  $\nu$  of interest. We repeat this process 1000 times. The resultant distribution of  $A_0, B_0$  at each frequency  $\nu$  represents what we would expect to find in a universe where ALPs do not exist. Each distribution is bivariate normal with some rotation angle. We rotate each distribution into the primary axes  $A', B'$  where the variance of the distribution is maximized along  $A'$  and minimized along  $B'$ , to define the no-ALP distribution (see [41] for more details):

$$\mathcal{N} = \frac{1}{2\pi\sigma_{A'}\sigma_{B'}} e^{-\frac{1}{2}\left(\frac{A'^2}{\sigma_{A'}^2} + \frac{B'^2}{\sigma_{B'}^2}\right)}. \quad (6)$$

We still need to determine the probability distributions in the case that ALPs do exist. Note that  $A'$  and  $B'$  are still random variables in this case due to the stochastic nature of the ALP field: different spatio-temporal modes of the field interfere with each other (the ALP field at any point in space is a sum over many contributions with random phases), so the field amplitude is stochastic over timescales longer than the coherence time [44, 45]. Except at the very high end of our analysis range, the ALP coherence time is much larger than the duration of our measurement, so we resolve only a single mode of the ALP field. In this limit the local ALP field may be written in the form

$$a(T) = \alpha \sqrt{\rho_{\text{DM}}}/m_a \cos(\omega T + \phi), \quad (7)$$

where  $\rho_{\text{DM}} = 0.4 \text{ GeV}/\text{cm}^3$  is the mean local dark matter density [46],  $\omega$  includes a small contribution from the ALP kinetic energy,  $\phi \in [0, 2\pi)$  is a uniform-distributed random variable, and  $\alpha \geq 0$  is a Rayleigh-distributed random variable:  $P(\alpha) = \alpha e^{-\alpha^2/2}$ . The modifications to our analysis due to the decoherence of the ALP field are discussed in our Supplemental Information [41], otherwise we assume  $\alpha$  and  $\phi$  are constant over the entire data collection time. The oscillating  $C_S$  term in the Ramsey fringe frequency is then written as

$$f^{C_S}(T) = 2W_S\eta C_G/f_a a(T), \quad (8)$$

where  $C_G/f_a$  is the ALP-gluon coupling and  $\eta \approx 0.03$  is a coefficient relating  $C_S$  induced in a generic heavy nucleus to the QCD theta angle [32, 47]. The quadrature amplitudes of the ALP signal are then

$$\begin{aligned} A' &= 2W_S\eta C_G/f_a \alpha \sqrt{\rho_{\text{DM}}}/m_a \cos(\phi) \\ B' &= -2W_S\eta C_G/f_a \alpha \sqrt{\rho_{\text{DM}}}/m_a \sin(\phi). \end{aligned} \quad (9)$$

As mentioned earlier,  $A'$  and  $B'$  must still be treated as random variables even in the absence of noise; the fact that  $\alpha$  is Rayleigh-distributed implies that  $A'$  and  $B'$  are each Gaussian distributed with mean zero and variance

$$\sigma_X^2 = (2W_S\eta C_G/f_a \sqrt{\rho_{\text{DM}}}/m_a)^2. \quad (10)$$

The equal quadrature variances reflect our ignorance of the local phase of the ALP field oscillations. The fact that  $A'$  and  $B'$  can simultaneously be small reflects the possibility that the earth may have been near a null in ALP density during our data collection time. We can now construct the expected ‘ALP distribution’ by adding the variance  $\sigma_X^2$  to our no-ALP variances (the no-ALP variances characterize the experimental noise). This defines a new bivariate normal distribution

$$\mathcal{X} = \frac{1}{2\pi\sigma_{AX}\sigma_{BX}} e^{-\frac{1}{2}\left(\frac{A'^2}{\sigma_{AX}^2} + \frac{B'^2}{\sigma_{BX}^2}\right)}, \quad (11)$$

which we call our ‘ALP distribution’. Here,  $\sigma_{AX}^2 = \sigma_{A'}^2 + \zeta\sigma_X^2$  and  $\sigma_{BX}^2 = \sigma_{B'}^2 + \zeta\sigma_X^2$ . We encapsulate sources of attenuation, including decoherence of the ALP field due to the finite linewidth, in the frequency-dependent factor  $\zeta$  which we discuss in detail in the Supplemental Information [41].

Now we can compare probabilities for the ALP vs no-ALP case. For each hypothesized coupling strength  $C_G/(f_a m_a)$  and frequency  $\nu$  of interest we take the ratio of the probability distributions  $\mathcal{N}$  and  $\mathcal{X}$  evaluated at our actual measured amplitudes  $A'_0$  and  $B'_0$ :

$$U_i(\nu_i, C_G/(f_a m_a)) = \frac{\mathcal{X}(A'_0(\nu_i), B'_0(\nu_i), \nu_i, C_G/(f_a m_a))}{\mathcal{N}(A'_0(\nu_i), B'_0(\nu_i), \nu_i)}, \quad (12)$$

which we call the *prior update*: the number  $U_i$  is a multiplicative factor which, when multiplied with our logarithmically-uniform priors, updates our prior belief to our post-experimental (or posterior) belief (see Figure 2). A 95% exclusion corresponds to the prior update dropping to 0.05 [43].

So far, our analysis has not taken into account the look-elsewhere effect. The colormap of  $U$  in Figure 2 simply shows how our belief in the existence of ALPs has changed as a function of frequency and coupling. To account for the look-elsewhere effect, owing to the fact that we are looking at more than  $10^6$  frequencies, we generate the *aggregate prior update*:

$$\mathcal{U}(C_G/(f_a m_a)) = \frac{\text{aggregate posterior}}{\text{aggregate prior}} = \frac{\sum_i U_i \epsilon/\nu_i}{\sum_i \epsilon/\nu_i}, \quad (13)$$

where  $\epsilon/\nu_i$  is our prior belief (for an ALP of frequency  $\nu_i$ ), using logarithmically-uniform priors ( $\epsilon$  being constant). We can sub-aggregate over any subset of the analysis range we like. The aggregate prior update taken over the *entire* set of frequencies analyzed represents the fractional change in our belief that an ALP of a given coupling strength exists anywhere in the full analysis range, which appropriately accounts for the look-elsewhere effect. The aggregate prior update as a function of coupling strength is plotted in Ref. [41].

Our results yield no strong indication of a dark matter signal over the range  $10^{-22} - 10^{-15}$  eV, so we use

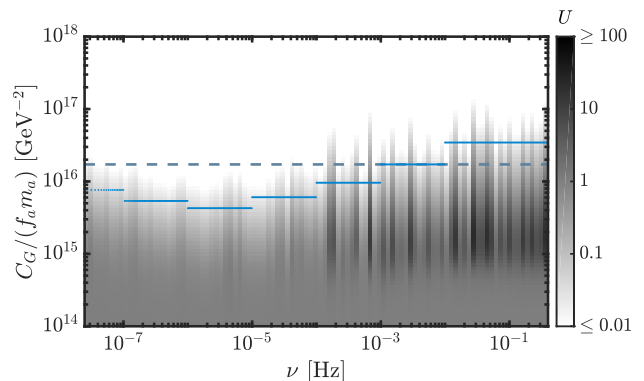


FIG. 2. Bayesian power measured analysis of the EDM data. The grayscale matrix corresponds to a sub-aggregation of the prior updates  $U$  over 100 logarithmically-spaced frequency bins. Darker shading on the logarithmic color scale corresponds to increased prior update, which can be interpreted as an increased belief in an ALP of given frequency  $\nu$  at ALP-gluon coupling  $C_G/(f_a m_a)$ . We use a blue line to indicate the 95% exclusion (which corresponds to the sub-aggregated update dropping to 0.05 [43]) for sub-aggregation over each decade. The corresponding greyscale matrix for this sub-aggregation is not shown. Finally, a dashed line corresponds to the aggregated exclusion over the full analysis range. The full un-aggregated matrix of  $U$  values is available upon request.

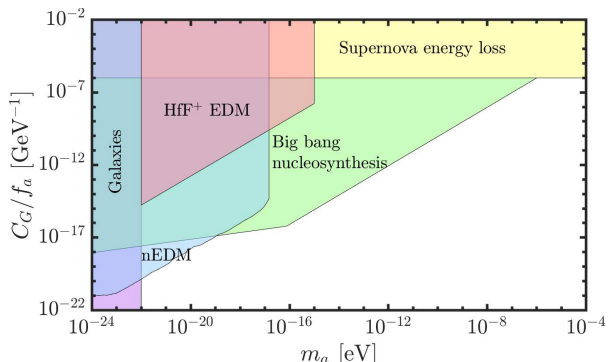


FIG. 3. Astrophysical and laboratory limits on the ALP-gluon interaction. All limits assume that ALPs saturate the local dark matter content. All constraints correspond to a 95% confidence level. The purple region embodies the constraint that the virial deBroglie wavelength is smaller than the size of a dwarf galaxy [26]. The blue region is the constraint derived from looking at neutron EDM oscillation [10]. The green region represents constraints from big bang nucleosynthesis [48], and the yellow region represents constraints from supernova energy loss bounds [49, 50]. The pink region is the constraint described in this work.

the above procedure to exclude  $C_G/f_a m_a > 1.72 \times 10^{16}$   $\text{GeV}^{-2}$  at 95% confidence. If we assume the density of the ALP field is held constant at its mean value, we can convert our exclusion back to frequency modulation amplitude in Hz via eq (7) and (8) which gives us an exclusion of 37 mHz. This is considerably less impressive-seeming than the limit of 1.2 mHz which we extracted from our original DC analysis [14]. This relaxation of

the exclusion is an unavoidable consequence of correctly accounting for the stochastic nature of the ALP field and the look-elsewhere effect associated with setting a limit across seven orders of magnitude in frequency.

Our constraint on the ALP-gluon coupling  $C_G/f_a$  is plotted in Figure 3 along with existing direct and indirect limits. Our results are the first laboratory constraints on the ALP-gluon coupling in the mass range  $10^{-17} - 10^{-15}$  eV.

The analysis techniques applied herein are general enough to apply to most time-series datastreams, and in particular will be applied to our next-generation EDM measurement which we expect to be about an order of magnitude more sensitive.

We thank E. J. Halperin, A. Derevianko and D. F. Jackson Kimball for enlightening discussions on the topic of ALPs. B. M. B. and Y. S. acknowledge support from National Research Council postdoctoral fellowships. V.F. acknowledges support from the Australian Research Council grants DP150101405 and DP200100150. W. B. C. acknowledges support from the Natural Sciences and Engineering Research Council of Canada. This work was supported by the Marsico Foundation, NIST, and the NSF (Grant No. PHY-1734006).

---

\* tanya.roussy@colorado.edu

† Present address: Department of Chemistry and Chemical Biology, Harvard University, 12 Oxford St, Cambridge MA 02138

‡ Present address: Honeywell Quantum Solutions, 303 S. Technology Ct., Broomfield, CO 80021, USA

§ Present address: Institute for Quantum Electronics, ETH Zürich, Otto-Stern-Weg 1, 8093 Zürich, Switzerland

¶ Present address: National Institute of Standards and Technology, 325 Broadway, Boulder, Colorado 80305, USA

\*\* Present address: Department of Physics and Astronomy, University of Nevada, Las Vegas, Las Vegas, NV 89154

- [1] M. E. Pospelov and I. B. Khriplovich, Electric-Dipole Moment of the W-Boson and the Electron in the Kobayashi-Maskawa Model, *Sov. J. Nuc. Phys.* **53**, 638 (1991).
- [2] M. S. Safronova, D. Budker, D. Demille, D. F. Kimball, A. Derevianko, and C. W. Clark, Search for new physics with atoms and molecules, *Reviews of Modern Physics* **90**, 25008 (2018).
- [3] M. Pospelov and A. Ritz, Electric dipole moments as probes of new physics, *Annals of Physics* **318**, 119 (2005).
- [4] Y. Nakai and M. Reece, Electric dipole moments in natural supersymmetry, *Journal of High Energy Physics* **2017**, 31 (2017).
- [5] J. Engel, M. J. Ramsey-Musolf, and U. Van Kolck, Electric dipole moments of nucleons, nuclei, and atoms: The Standard Model and beyond, *Progress in Particle and Nuclear Physics* **71**, 21 (2013).
- [6] E. M. Purcell and N. F. Ramsey, On the Possibility of Electric Dipole Moments for Elementary Particles and Nuclei, *Physical Review* **78**, 807 (1950).
- [7] J. H. Smith, E. M. Purcell, and N. F. Ramsey, Experimental limit to the electric dipole moment of the neutron, *Physical Review* **108**, 120 (1957).
- [8] D. Budker, P. W. Graham, M. Ledbetter, S. Rajendran, and A. O. Sushkov, Proposal for a cosmic axion spin precession experiment (CASPER), *Physical Review X* **4**, 1 (2014).
- [9] P. W. Graham and S. Rajendran, Axion dark matter detection with cold molecules, *Physical Review D* **84**, 055013 (2011).
- [10] C. Abel *et al.*, Search for axionlike dark matter through nuclear spin precession in electric and magnetic fields, *Physical Review X* **7**, 1 (2017).
- [11] C. T. Hill, Axion induced oscillating electric dipole moments, *Physical Review D* **91**, 111702 (2015).
- [12] V. V. Flambaum, B. M. Roberts, and Y. V. Stadnik, Comment on "axion induced oscillating electric dipole moments", *Physical Review D* **95**, 1 (2017).
- [13] Y. V. Stadnik and V. V. Flambaum, Axion-induced effects in atoms, molecules, and nuclei: Parity nonconservation, anapole moments, electric dipole moments, and spin-gravity and spin-axion momentum couplings, *Physical Review D* **89**, 1 (2014).
- [14] W. B. Cairncross, D. N. Gresh, M. Grau, K. C. Cossel, T. S. Roussy, Y. Ni, Y. Zhou, J. Ye, and E. A. Cornell, Precision Measurement of the Electron's Electric Dipole Moment Using Trapped Molecular Ions, *Physical Review Letters* **119**, 1 (2017).
- [15] P. A. R. Ade *et al.* (Planck Collaboration), Planck 2015 results. XIII. Cosmological parameters, *Astronomy & Astrophysics* **594**, A13 (2016).
- [16] D. J. Marsh, Axion cosmology, *Physics Reports* **643**, 1 (2016).
- [17] R. D. Peccei and H. R. Quinn, CP conservation in the presence of pseudoparticles, *Physical Review Letters* **38**, 1440 (1977).
- [18] R. D. Peccei and H. R. Quinn, Constraints imposed by CP conservation in the presence of pseudoparticles, *Physical Review D* **16**, 1791 (1977).
- [19] F. Wilczek, Problem of strong P and T invariance in the presence of instantons, *Physical Review Letters* **40**, 279 (1978).
- [20] S. Weinberg, A New Light Boson?, *Physical Review Letters* **40**, 223 (1978).
- [21] A. Arvanitaki, S. Dimopoulos, S. Dubovsky, N. Kaloper, and J. March-Russell, String axiverse, *Physical Review D* **81**, 123530 (2010).
- [22] M. Dine and W. Fischler, The not-so-harmless axion, *Physics Letters B* **120**, 137 (1983).
- [23] L. Abbott and P. Sikivie, A cosmological bound on the invisible axion, *Physics Letters B* **120**, 133 (1983).
- [24] J. Preskill, M. B. Wise, and F. Wilczek, Cosmology of the invisible axion, *Physics Letters B* **120**, 127 (1983).
- [25] W. Hu, R. Barkana, and A. Gruzinov, Fuzzy Cold Dark Matter: The Wave Properties of Ultralight Particles, *Physical Review Letters* **85**, 1158 (2000).
- [26] A. Derevianko, Detecting dark-matter waves with a network of precision-measurement tools, *Physical Review A* **97** (2018).
- [27] H.-Y. Schive, T. Chiueh, and T. Broadhurst, Cosmic structure as the quantum interference of a coherent dark

- wave, *Nature Physics* **10**, 496 (2014).
- [28] L. Hui, J. P. Ostriker, S. Tremaine, and E. Witten, Ultralight scalars as cosmological dark matter, *Physical Review D* **95**, 043541 (2017).
- [29] A. K. Drukier, K. Freese, and D. N. Spergel, Detecting cold dark-matter candidates, *Physical Review D* **33**, 3495 (1986).
- [30] Y. V. Stadnik (unpublished calculations).
- [31] V. V. Flambaum and H. B. Tran Tan, Oscillating nuclear electric dipole moment induced by axion dark matter produces atomic and molecular EDM, *Physical Review D* **100**, 111301 (2019).
- [32] V. V. Flambaum, M. Pospelov, A. Ritz, and Y. V. Stadnik, Sensitivity of EDM experiments in paramagnetic atoms and molecules to hadronic CP violation, arxiv:1912.13129 (2019).
- [33] V. V. Flambaum, I. B. Samsonov, and H. B. Tran Tan, Limits on CP-violating hadronic interactions and proton EDM from paramagnetic molecules, arxiv:2004.10359 (2020).
- [34] The authors of [32, 33] calculate the magnitude of the scalar-pseudoscalar electron-nucleon coupling  $C_S$  that would be generated by a heavy nucleus like Hf by a nonzero QCD  $\theta$  parameter. An ALP coupled to gluons behaves like a dynamical version of  $\theta_{\text{QCD}}$ , and thus generates an oscillating  $C_S$ .
- [35] Here,  $m_F$  refers to the Zeeman sublevel and  $\Omega$  refers to the projection of the sum of electronic and rotational angular momentum onto the molecular axis.
- [36] T. Fleig and M. Jung, Model-independent determinations of the electron EDM and the role of diamagnetic atoms, *Journal of High Energy Physics* **2018**, 12 (2018).
- [37]  $\mathcal{A}_i$  is positive when we prepare the same state as we read out, and negative when we prepare the opposite state to the one we read out.
- [38] In our previous constraint of the static eEDM, we used a slightly different asymmetry, which required 2 shots to collect:  $\mathcal{A} = \frac{N_{\uparrow} - N_{\downarrow}}{N_{\uparrow} + N_{\downarrow}}$ , where  $N_{\uparrow/\downarrow}$  indicates the number of  $\text{Hf}^+$  molecules we counted from the  $m_F = \pm 3/2$  stretched states, respectively. For this analysis, we use a ‘single-shot definition instead, as it allows us to extend our analysis band out to 400 mHz.
- [39] E. R. Meyer, A. E. Leanhardt, E. A. Cornell, and J. L. Bohn, Berry-like phases in structured atoms and molecules, *Physical Review A - Atomic, Molecular, and Optical Physics* **80**, 10.1103/PhysRevA.80.062110 (2009).
- [40] The reader would be justified to scoff at calling  $\mu\text{Hz}$  to mHz ‘high frequency’, but we beg their patience.
- [41] See Supplemental Material.
- [42] If one searches a large area in parameter space for some effect (in our case, over  $10^6$  possible ALP frequencies for an oscillation signal), one is bound to see a statistical fluctuation. The look-elsewhere effect is the name for this phenomenon: if one continues to look elsewhere, they may find what they are looking for.
- [43] D. A. Palken *et al.*, Improved analysis framework for axion dark matter searches, *Phys. Rev. D* **101**, 123011 (2020).
- [44] G. P. Centers *et al.*, Stochastic amplitude fluctuations of bosonic dark matter and revised constraints on linear couplings (2019), arXiv:1905.13650.
- [45] J. W. Foster, N. L. Rodd, and B. R. Safdi, Revealing the dark matter halo with axion direct detection, *Physical Review D* **97**, 123006 (2018).
- [46] R. Catena and P. Ullio, A novel determination of the local dark matter density, *Journal of Cosmology and Astroparticle Physics* **2010** (8).
- [47] We expect forthcoming nucleus-specific calculations to improve the inferred sensitivity [33].
- [48] K. Blum, R. T. D’Agnolo, M. Lisanti, and B. R. Safdi, Constraining axion dark matter with Big Bang Nucleosynthesis, *Physics Letters, Section B: Nuclear, Elementary Particle and High-Energy Physics* **800**, 130001 (2020).
- [49] P. W. Graham and S. Rajendran, New observables for direct detection of axion dark matter, *Physical Review D - Particles, Fields, Gravitation and Cosmology* **80**, 085017 (2009).
- [50] G. G. Raffelt, Astrophysical methods to constrain axions and other novel particle phenomena, *Physics Reports* **198**, 1 (1990).

# Experimental constraint on axion-like particle coupling over seven orders of magnitude in mass: Supplemental Material

Tanya S. Roussy,<sup>1,2,\*</sup> Daniel A. Palken,<sup>1,2</sup> William B. Cairncross,<sup>1,2,†</sup> Benjamin M. Brubaker,<sup>1,2</sup>  
 Daniel N. Gresh,<sup>1,2,‡</sup> Matt Grau,<sup>1,2,§</sup> Kevin C. Cossel,<sup>1,2,¶</sup> Kia Boon Ng,<sup>1,2</sup> Yuval Shagam,<sup>1,2</sup>  
 Yan Zhou,<sup>1,2,\*\*</sup> Victor V. Flambaum,<sup>3,4</sup> Konrad W. Lehnert,<sup>1,2</sup> Jun Ye,<sup>1,2</sup> and Eric A. Cornell<sup>1,2</sup>

<sup>1</sup>*JILA, NIST and University of Colorado, Boulder, Colorado 80309, USA*

<sup>2</sup>*Department of Physics, University of Colorado, Boulder, Colorado 80309, USA*

<sup>3</sup>*School of Physics, University of New South Wales, Sydney 2052, Australia*

<sup>4</sup>*Johannes Gutenberg University of Mainz, 55128 Mainz, Germany*

(Dated: July 2, 2020)

## FREQUENCY RANGES

Our analysis was broken into two regimes: ‘low frequency’ (27 nHz – 126  $\mu$ Hz) and ‘high frequency’ (126  $\mu$ Hz – 400 mHz). The fundamental limits of the low frequency analysis were set by the inverse timespan of the entire dataset (27 nHz, see Figure 1a) and the ‘Nyquist’ limit for the ‘block’ collection (each block took 22 minutes to collect, so this is 378  $\mu$ Hz). The fundamental lower limit of the high frequency analysis was set by the inverse timespan of the most sensitive data, which was taken over an 11-day period in 2017 (1.12  $\mu$ Hz, see Figure 1b). The upper limit is slightly below the ‘Nyquist’ limit – each point took about 1 second to collect and we chose 400 mHz. Our data is not evenly spaced in time, so we are using the term ‘Nyquist limit’ in a loose sense: with unevenly spaced data, the Nyquist frequency is often *higher* than one might expect [1]. The frequency ranges above have considerable overlap,

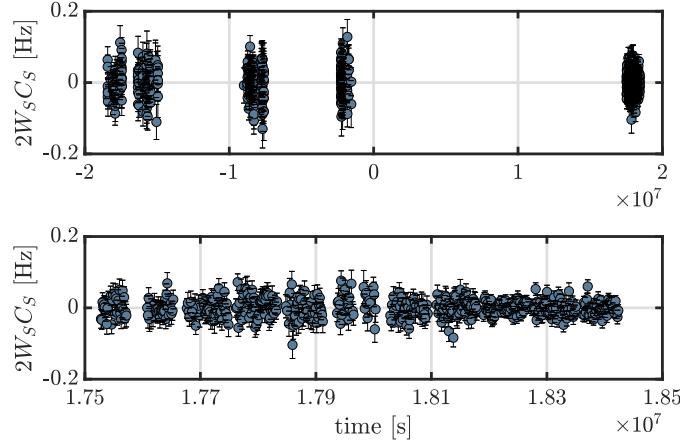


FIG. 1. (Top) Individual  $C_S$  measurements plotted as a function of their acquisition time since August 15 2016 (the temporal ‘center’ of our dataset). (Bottom) Our most sensitive  $C_S$  measurements were collected over 11 days in 2017. For the low frequency analysis we used the entire dataset (top), and for the high frequency analysis we used only the most sensitive 11 days (bottom).

and we used this overlap to validate our high frequency analysis. We analyzed the same dataset using both the ‘low frequency’ and ‘high frequency’ methods and found virtually the same LSSA result in both cases. Taken together, the entire dataset was enormous, so we chose to truncate both datasets to eliminate overlap and reduce the size of the dataset, which made computing slightly less resource-intensive.

## TIMESTAMP SHUFFLING

As described in the main text, our statistical analysis requires simulated data which, by construction, contains no coherent oscillations in the  $f^{C_S}$  channel. For the low-frequency analysis this is a rather simple procedure which relies

on our knowledge that each block-based  $f^{Cs}$  measurement is drawn from a Gaussian distribution with mean zero and well-characterized variance [2]. For the high-frequency analysis our simulation technique warrants further discussion.

The challenge is to simulate shot-by-shot data which preserves the basic structure of the fringes and blocks as well as the inherent noise of the measurements. The fringes themselves have a coherent oscillation in them, and each block contained eight fringes – each of which may oscillate at a slightly different frequency depending on the switch state. The fringes also had a limited coherence time, which varied throughout the dataset as we changed experimental parameters. While generating simulated data that faithfully preserves these features is in principle possible, the most difficult part for our purposes was preserving the noise. There were a number of technical noise sources which were not easily characterized, i.e. they didn’t conform to some known distribution, and were transient, i.e. they were present or absent to different degrees through the dataset.

We found that the most effective way to preserve the qualitative features of the noise and the specific details of the fringes and blocks while erasing any real-time coherent oscillation in the  $f^{Cs}$  channel was to randomly shuffle the timestamps of the data by block. As described in the main text, a block of data formed one single  $f^{Cs}$  measurement and was composed of eight Ramsey fringes, which together comprise 96 data points, or 1536 shots. When we collected a block of data we would *not* collect each Ramsey fringe one at a time, slowly increasing the free-evolution time until completion then changing the switch state to collect the next fringe. Instead, we would increase the Ramsey time while scrambling the various switch states, effectively collecting points from each fringe in random order. In other words, we randomized the order in which we collected the 96 data points corresponding to each block, such that there is no fixed relationship between either the switch state or Ramsey time of adjacent data points. When we shuffle the timestamps by block, that means we take all timestamps of the data points belonging to a given block and swap them with timestamps for data points belonging to some other block. One can imagine this as swapping whole blocks around in time. Since a block corresponds to a  $f^{Cs}$  measurement, this will eliminate any coherent oscillation in the  $f^{Cs}$  channel which may have been present.

It is clear why shuffling the timestamps by block should erase any oscillations on the timescale of the block itself or longer, but it may not be clear why the technique works for oscillations with a higher frequency. The reason this works is due to the manner in which the data was collected – the random scrambling of when we collected the Ramsey times and switch states is unique to every block, so the shuffle introduces phase jumps into the data on the timescale of single data points – in other words, it effectively shuffles the data on the *data point* (16 second) timescale.

One might ask: why not just shuffle the timestamps by data point? The reason is that shuffling by data point, while very effective at erasing any coherent oscillation present, also appears to drastically change the spectral structure of the noise in our dataset. One might then ask why we don’t simply simulate the data directly, and again we find that assuming a specific noise model (such as shot noise in the HFF<sup>+</sup> count) is insufficient for simulating the real noise we had present. It should go without saying that arbitrarily increasing the noise in the simulated data led to the risk of hiding any real oscillation which would otherwise be detected, has no real scientific basis, and should be avoided.

To confirm that our simulation method really did sufficiently attenuate coherent oscillations while preserving the spectral structure of the noise in our dataset, we performed least-squares spectral analysis (LSSA) on simpler versions of simulated datasets which by construction contained a coherent oscillation as well as noise. The simulated data was sampled at the same times as our real dataset, and we performed simulations at frequencies throughout the bandwidth analyzed. In each case we found that the detected amplitude of the oscillation was significantly attenuated while the noise at other frequencies was not affected. Conversely, when we shuffled by data point or shot we found that while any coherent oscillation would be erased, the noise at other frequencies would also be attenuated.

## ESTIMATING THE NO-ALP DISTRIBUTION

Our analysis hinges on having a good estimate of the no-ALP distribution, which itself relies on knowing the variances  $\sigma_{A'}^2$  and  $\sigma_{B'}^2$ . Because we are searching over such a large frequency range, and examining so many different frequencies, there are many upward fluctuations in the oscillation amplitudes obtained from LSSA. Small fluctuations in the estimated variances can result in large changes in the apparent significance of these amplitudes. If our estimates of  $\sigma_{A'}^2$  and  $\sigma_{B'}^2$  are poor, our exclusion will reflect that.

One might think that the best way to ensure we have good estimates of the variances would be to do many more simulations. Unfortunately, especially for the high frequency data, the simulations were very computationally expensive so running more simulations was not an option. Because we only ran 1000 simulations our error in estimating the variances is dominated by statistical noise. To account for this, we chose to adjust the raw variances obtained from the simulated data to better match what we know to be true.

In the low frequency range, we made no adjustments to the variances. We know that there will be some phases



and frequencies which are favoured due to the temporal structure of the data (see Figure 1, top), so we wanted to preserve any structure in the variances which we found via simulation (including significant differences between the two quadratures  $A', B'$ ), even if it was a bit more noisy than desired due to the limited number of simulations.

In contrast, for the high frequency range we have no reason to believe there would be any meaningful difference between the two quadratures thanks to the near-continuous temporal spacing of the data we analyze (see Figure 1, bottom). In addition, we know that statistical fluctuations are independent, bin-to-bin. So to attenuate the effect of statistical fluctuations we smoothed the data using a 36-bin running average (this is 6 times our spectral resolution) and then averaged the the two quadratures  $A', B'$ . We chose 36 bins as we would expect a real fluctuation to span about 6 bins, so it would be roughly maintained over a 36 bin average, while a fake (statistical) fluctuation would only span 1 bin, so it would be strongly attenuated with a 36 bin average. We believe these are well-justified methods to prevent random fluctuations from affecting our analysis.

## SOURCES OF ATTENUATION

To reduce the risk of artificially over-constraining the axion-like particle (ALP) coupling it was important to account for all the known sources of attenuation present in our experimental signal. To date we are aware of three possible sources of attenuation:

1. When the total observation time  $T$  is smaller than the coherence time  $\tau_c$ , i.e.  $T < \tau_c$ , the ALP field is built from a sum over many phases of a freely oscillating bosonic field in three dimensions, resulting in a random distribution of the field amplitude. We must account for the probability that the local ALP field amplitude is significantly smaller than its RMS value throughout the galaxy. For example it is possible that when we took the data we could have been, by sheer bad luck, be sitting near a null of the field [3].
2. When the total observation time  $T$  is comparable to the coherence time  $\tau_c$ , i.e.  $T \sim \tau_c$ , decoherence due to the finite linewidth of the ALP field will decrease the measured signal amplitude [4].
3. When the observation time for a given *sample* (i.e. a block in the low frequency analysis or a shot in the high frequency analysis) is not small compared to the period of the ALP-induced oscillation, we are effectively averaging over some portion of the wave, leading to attenuation of the signal.

### Effect 1: Random distribution of the ALP field amplitude

This effect is dealt with automatically in the Bayesian Power Measured analysis framework. When we generate the ALP distribution  $\mathcal{X}$  from the no-ALP distribution  $\mathcal{N}$  we we increase the variance of both quadratures without increasing the mean. See the main text between equations (7)-(11) for more details.

### Effect 2: Decoherence

To quantify the effect of decoherence we compared a realistic (finite linewidth) ALP field to an infinitely narrow linewidth field at several possible mass values. We built the realistic field from its constituent parts as described in Ref. [4], implementing eqs (3) – (10) numerically. The result is an expression for the local ALP field, which we can ‘fit’ using LSSA as described in the main text. To generate the ‘infinitely narrow’ ALP distribution, we follow the same steps but instead sample the velocity distribution only once, then build up the full field. We ‘fit’ this field with LSSA as well, then repeat the process hundreds of times to get distributions for the quadrature amplitudes  $A_0, B_0$  in both cases. We call the amplitudes  $A, B$  and  $A_{\text{narrow}}, B_{\text{narrow}}$ . We rotate these distributions into the primary axes where the variance is maximized along one axis, then define the attenuation due to decoherence in each quadrature  $\zeta_{d,i}$  as the ratio of the variances:  $\zeta_{d,A} = \sigma_A^2 / \sigma_{A,\text{narrow}}^2$ ,  $\zeta_{d,B} = \sigma_B^2 / \sigma_{B,\text{narrow}}^2$ . In practice we find  $\zeta_{d,A} \sim \zeta_{d,B}$ , so we define  $\zeta_d = (\zeta_{d,A} + \zeta_{d,B}) / 2$ . Unsurprisingly we see no decoherence effect in our low frequency band, but we do at the extreme high end of the high frequency band. We fit the results using a second-order polynomial to obtain a functional form for the attenuation due to decoherence over the entire analysis band:  $\zeta_d(\nu)$  (Figure 2).

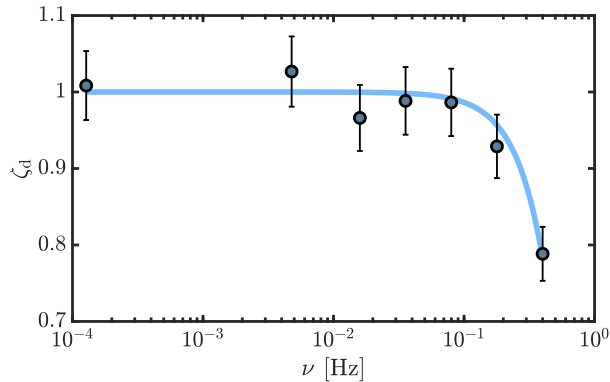


FIG. 2. Attenuation factor due to ALP field decoherence, calculated over the high frequency analysis range. Grey-filled circles are the calculated values, and the blue curve is the fit.

### Effect 3: Finite sample time

At the high end of each analysis regime, we are analyzing frequencies high enough that there is a non-negligible change in the signal during the sample time  $t_R$ . This results in an ‘averaging’ of the oscillation over the sample time and an effective attenuation in perceived signal amplitude. For instance, at the upper end of our high frequency range we analyze 0.4 Hz but each sample takes about one second to acquire. We have a similar issue at the high frequency end of the low frequency analysis. To quantify this attenuation, we generated artificial sinusoidal data sampled more finely than the timestamps in our real dataset, then averaged the signal over the actual intervals of data collection. We did this for a number of frequencies spaced through our analysis band, then averaged these results over phases spanning  $[0, 2\pi)$ . We then perform LSSA on both the original simulated data and the averaged simulated data and define the attenuation due to finite sample time  $\zeta_{s,i}$  in each quadrature as  $\zeta_{s,A} = \sigma_A^2 / \sigma_{A'}^2$ ,  $\zeta_{s,B} = \sigma_B^2 / \sigma_{B'}^2$ , where  $A, B$  are from the averaged signal and  $A', B'$  are from the original signal. We average the two quadrature attenuation factors to determine the attenuation due to finite sample time  $\zeta_s$ . We did this for both the high frequency analysis and the low frequency analysis, and used the fits to the data to generate a piecewise function describing the attenuation due to this effect as a function of frequency (Figure 3).

Finally, our overall attenuation factor over the entire analysis band is given by the product of the attenuation factors for the two effects:  $\zeta(\nu) = \zeta_d(\nu)\zeta_s(\nu)$ . This is the quantity introduced below Eq. (7) in the main text.

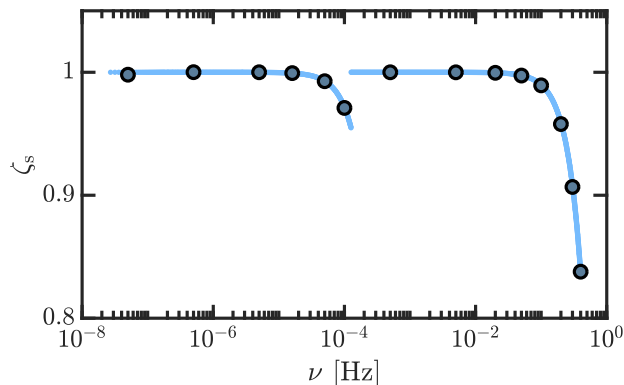


FIG. 3. Attenuation due to finite sample time over the entire analysis range. The blue curve shows the piecewise function generated by the fit to the grey circles.

## AGGREGATE PRIOR UPDATE

As described in the main text, the aggregate prior update (Figure 4) describes the fractional change in our belief that an ALP of a given coupling strength exists *anywhere* in the full analysis range, which accounts for the look-elsewhere effect.

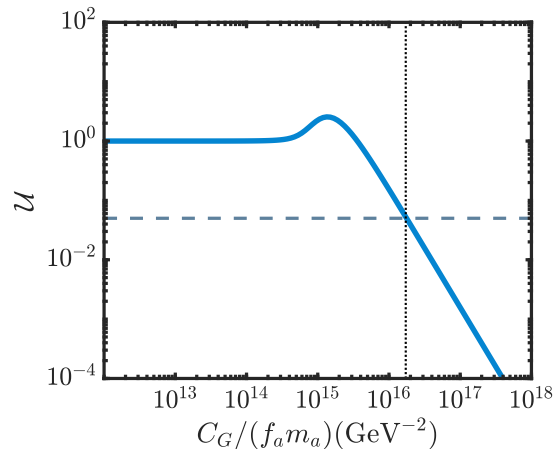


FIG. 4. Aggregate prior update  $\mathcal{U}$  (equivalently, exclusion) as a function of ALP-gluon coupling  $C_G/(f_a m_a)$ . The horizontal dotted line indicates 95% exclusion, while the vertical dotted line indicates the lower limit of  $C_G/(f_a m_a)$  which is excluded at 95% confidence over the entire analysis band. Had our data presented us with strong affirmative evidence for the existence of an ALP in our frequency range, the curve of  $\mathcal{U}$  vs  $C_G/(f_a m_a)$  might have peaked not at  $\mathcal{U} = 2.5$  but for instance at  $\mathcal{U} = 1, 000$  or higher.

---

\* tanya.roussy@colorado.edu

† Present address: Department of Chemistry and Chemical Biology, Harvard University, 12 Oxford St, Cambridge MA 02138

‡ Present address: Honeywell Quantum Solutions, 303 S. Technology Ct., Broomfield, CO 80021, USA

§ Present address: Institute for Quantum Electronics, ETH Zürich, Otto-Stern-Weg 1, 8093 Zürich, Switzerland

¶ Present address: National Institute of Standards and Technology, 325 Broadway, Boulder, Colorado 80305, USA

\*\* Present address: Department of Physics and Astronomy, University of Nevada, Las Vegas, Las Vegas, NV 89154

- [1] L. Eyer and P. Bartholdi, Variable stars: Which Nyquist frequency?, *Astronomy and Astrophysics Supplement Series* **135**, 1 (1999).
- [2] W. B. Cairncross, D. N. Gresh, M. Grau, K. C. Cossel, T. S. Roussy, Y. Ni, Y. Zhou, J. Ye, and E. A. Cornell, Precision Measurement of the Electron's Electric Dipole Moment Using Trapped Molecular Ions, *Physical Review Letters* **119**, 1 (2017).
- [3] G. P. Centers *et al.*, Stochastic amplitude fluctuations of bosonic dark matter and revised constraints on linear couplings (2019), arXiv:1905.13650.
- [4] J. W. Foster, N. L. Rodd, and B. R. Safdi, Revealing the dark matter halo with axion direct detection, *Physical Review D* **97**, 123006 (2018).